Am J Transl Res 2026;18(8):6662-6671
www.ajtr.org /ISSN:1943-8141/AJTR0170697

Original Article

A *CHD7* intronic variant induces aberrant splicing and structural alterations in the CHD7 DNA-binding domain to cause CHARGE syndrome

Yangfan Fei[1,2*], Dan Hu[1,2*], Lyu Liu[1,2], Xianglian Tian[3], Jinbao Chai[1,2], Lixia Wu[1,2], Aiping Li[1,2], Qinglian Zhang[3], Daibo Li[1,4]

[1]West China Hospital Sichuan University, Meishan Hospital, Meishan, Sichuan, China; [2]Department of Endocrinology and Metabolism, Meishan People's Hospital, Meishan, Sichuan, China; [3]School of Laboratory Medicine, Chengdu Medical College, Chengdu, Sichuan, China; [4]Department of Otolaryngology, Meishan People's Hospital, Meishan, Sichuan, China. [*]Equal contributors.

Received December 12, 2025; Accepted June 8, 2026; Epub August 15, 2026; Published August 30, 2026

Abstract: Objectives: CHARGE syndrome (CS), a rare inherited condition, is mainly caused by pathogenic variants in the gene encoding chromodomain helicase DNA-binding protein 7 (*CHD7*). In the present investigation, the genetic etiology of CS was elucidated in a Chinese patient presenting with characteristic clinical features. Methods: A 28-year-old female with amenorrhea, facial asymmetry, right ear malformation, hearing impairment, and congenital cardiac anomalies was evaluated using whole-exome sequencing (WES) for mutation screening. Familial Sanger sequencing subsequently confirmed the identified variant as *de novo*. Minigene assays were used to assess the pathogenicity of the splicing variant, while the structural alterations in CHD7 were characterized using computational modeling and electrostatic potential analyses. Results: WES detected a heterozygous *CHD7* splice-site variant, c.5405-17 G>A, which was not detected in either parent. Minigene-based functional assessments revealed this *de novo CHD7* variant to cause a 15-bp insertion, resulting in a five-amino-acid insertion between the helicase and the SANT domains of CHD7, thereby potentially altering DNA binding. Hormone replacement therapy successfully induced cyclic menstruation, and surgical intervention corrected the auricular deformity. Conclusions: A *de novo* pathogenic splice-site mutation (c.5405-17 G>A) was identified in this study, which leads to the pathogenesis of CS. Subsequent functional evaluation confirmed that this mutation disrupts normal mRNA processing, thereby inducing structural alterations in the CHD7 protein. The results obtained herein advance our understanding of the mutational spectrum of *CHD7*, while emphasizing the importance of combining clinical, genetic, and functional analyses for the definitive diagnosis of CS.

Keywords: CHARGE syndrome, *CHD7* gene, whole-exome sequencing, splice-site variant, homology modeling, *de novo* mutation

Introduction

CHARGE syndrome (CS; OMIM 214800), a rare congenital disorder characterized by a wide spectrum of abnormalities [1], has an estimated prevalence of approximately 1 in 8,500-12,000 live births worldwide [2]. Following its first description and characterization by Hall in 1979 [3], the acronym CHARGE was introduced in 1981 by Pagon et al. to denote its primary clinical manifestations, including ocular coloboma, cardiac anomalies, choanal atresia, growth and/or developmental retardation, genitourinary malformations and/or hypogonadism, and auricular abnormalities and/or hearing impairment [4]. At present, CS is predominantly diagnosed through clinical evaluation, with molecular testing increasingly recognized as a valuable tool for diagnostic confirmation. Pathogenic variants in the gene encoding chromodomain helicase DNA-binding protein 7 (*CHD7*; OMIM: 608892) are frequently associated with CS, a congenital condition exhibiting autosomal dominant inheritance [5]. A 2010 study enroll-

https://doi.org/10.62347/UFCX1012

ing 379 individuals diagnosed with CS detected pathogenic *CHD7* variants in 67% of cases through genetic analyses of *CHD7* [6].

The 188 kb-long *CHD7* gene, located on chromosome 8 (8q12.2), consists of 42 exons and encodes the CHD7 protein, which functions as a transcriptional regulator involved in ATP-dependent chromatin remodeling and epigenetic regulation. CHD7 belongs to an evolutionarily conserved group of nucleoproteins that exhibit ATP-dependent chromatin remodeling activity [7]. CHD7 interacts with the polybromo- and BRG1 (Brahma-related gene 1)-associated factor-containing complex (PBAF) to form a functional unit that modulates chromatin architecture, regulates gene transcription, and influences embryonic development in human neural crest cells [8, 9]. *CHD7* mutations have been detected in 65-70% of patients diagnosed with CS [10-12]. A previous study also identified a mutation in the semaphorin 3E gene (*SEMA3E*) in a patient with CS [13]. A broad spectrum of *CHD7* mutations has been extensively documented to date, including missense and nonsense variants, splice-site alterations, frameshift mutations caused by deletions or insertions, as well as large-scale deletions, duplications, and translocations. Of these mutations, splice-site variants represent a distinct challenge for both diagnostic assessment and functional interpretation. The pathogenicity of canonical splice-site mutations affecting invariant GT/AG dinucleotides is readily recognized; however, the clinical significance of deep intronic variants often remains unclear without functional validation [14, 15]. By creating or activating cryptic splice sites, these variants can lead to aberrant mRNA processing and the production of nonfunctional proteins; however, they are often overlooked or classified as variants of uncertain significance (VUS) in routine exome sequencing studies [16].

The present report describes the case of a 28-year-old female presenting with atypical pubertal development accompanied by several congenital anomalies, including craniofacial, spinal, auditory, and cardiac abnormalities. Whole-exome sequencing (WES) with next-generation sequencing (NGS) was implemented in this study to identify a splice-site variant, c.5405-17 G>A, in the *CHD7* gene in this patient, who was diagnosed with severe CS. By employing minigene assays, we subsequently assessed the pathogenicity of the c.5405-17 G>A variant for determining its functional effects, which led to the detection of an in-frame insertion of five amino acids in the CHD7 protein, thereby indicating its role in the pathogenesis of CS.

Materials and methods

The study workflow is outlined in **Figure 1**.

Patient presentation and clinical features

The patient was recruited from Meishan People's Hospital, and her comprehensive clinical data, including general health status, present illness, past medical and family histories, physical examination findings, ancillary investigations, and treatment course, were collected and analyzed systematically. Peripheral blood samples were obtained for DNA extraction and WES analyses, following which Sanger sequencing was conducted for validation of the identified variants.

WES and data analyses

Peripheral blood samples were collected from the proband and her parents in anticoagulant tubes with EDTA. Genomic DNA was subsequently extracted from the samples using the commercial Blood Genomic DNA Extraction Kit (TIANGEN Biotech, Beijing, China) and WES was performed by Shanghai We-Health Biomedical Technology Co., Ltd., China. Library preparation was performed using the Hieff NGS® OnePot DNA Library Prep Kit for Illumina® (YEASEN Biotech, Shanghai, China), followed by clinical exome capture with a custom capture panel from Twist Bioscience Corporation (USA). The enriched libraries were sequenced on the DNBSEQ-T7 platform (MGI Tech, Shenzhen, China) in paired-end 100 bp mode. The raw sequencing reads were initially aligned to the reference genome (GRCh38/hg19) using the Burrows-Wheeler Aligner (BWA) algorithm and subsequently processed with SAMtools. The cleaned reads were then remapped to the reference genome with BWA, and variant identification was performed using the Genome Analysis Toolkit (GATK v3.70).

Sanger sequencing

Genomic DNA was extracted from the peripheral blood samples using the TIANamp Blood

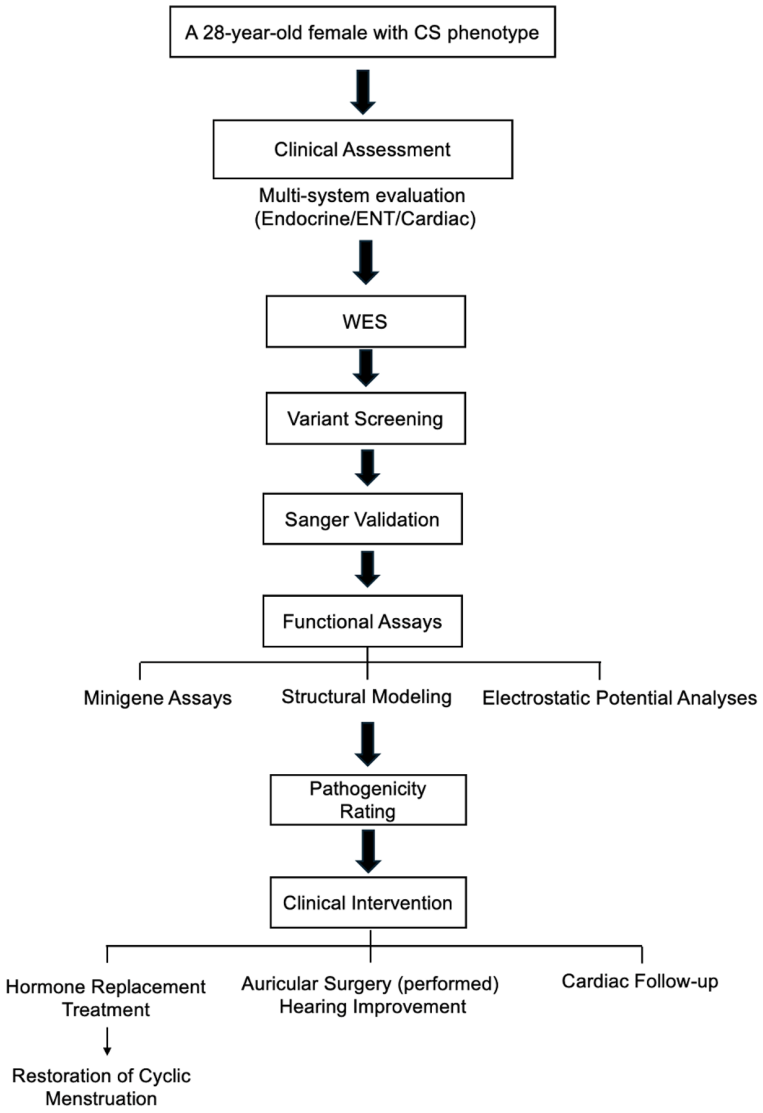

Figure 1. Study workflow. CS, CHARGE syndrome; ENT, ear, nose and throat; WES, whole-exome sequencing.

DNA Kit (TIANGEN Biotech, Beijing, China). Primer design was performed using Primer3Plus software (http://www.primer3plus.com/cgibin/dev/primer3plus.cgi), and the sequences of the forward and reverse primers were as follows: CHD7-c5428-Forward primer: GGATTCAACAGAGATGCTAACCTT; CHD7-c5428-Reverse primer: CCTTCTTACCCGTCACCACC. Polymerase chain reaction (PCR) amplification was performed in 20 mL reaction volumes using primers with an annealing temperature of 60°C. The thermal cycling conditions consisted of an initial step at 95°C for 1 minute, followed by 35 cycles of denaturation at 94°C for 30 seconds and annealing/extension at 60°C for 40 seconds, and the final extension at 60°C for 3 minutes. The PCR products were analyzed by 2% agarose gel electrophoresis, purified, and directly sequenced using an ABI3730xl DNA Analyzer (Applied Biosystems, Foster City, California, USA).

Minigene assay

The functional impact of the *de novo CHD7* splice-site variant (c.5405-17 G>A) was assessed through *in vitro* splicing assays. The wild-type (WT) and mutant (MT) *CHD7* constructs consisted of exon 25, intron 26, exon 27, and a segment of intron 25. These segments were subjected to PCR amplification with specific primers from a control individual and the proband. The primer sequences were as follows: forward primer (CHD7-F): 5'-AAGCTTGGTACCGAGCTCGGATCCTG-AAGCCGATGTGTGGATCCCTGAACCT-3'; reverse primer (CHD7-R): 5'-TTAAACGGGCCCTCTAGACTC-GAGATCTATTTCATCTTTGAACGGTGTTCTG-3'; MT forward primer (CHD7-MT-F): 5'-TTCTGTGCA-CaGATGGGCACGGCACAGGCTAT-3'; and MT reverse primer (CHD7-MT-R): 5'-CCCATCtGTGCACAGAA-AACACACAGAAACAA-3'. The amplified products were subjected to purification and subsequent digestion with the restriction enzymes BamHI and XhoI, followed by cloning into a linearized pMini-CopGFP vector and transformation into TOP10-competent cells. Constructs containing either the MT or WT sequences were verified by Sanger sequencing and subsequently transfected into HEK293T cells. An empty vector and mock transfection were included as controls. The cells that had undergone successful transfection were harvested after 48 h of transfection for subsequent RNA extraction. Total RNA was extracted using the miRNeasy Mini Kit (Qiagen, Venlo, The Netherlands), and approximately 1 μg of RNA was reverse-transcribed into cDNA using the

High Capacity RNA-to-cDNA Kit (TIANGEN Biotech, Beijing, China), following the manufacturer's instructions.

The resulting cDNA was subjected to PCR amplification using specific forward (MiniRT-F: 5'-GGCTAACTAGAGAACCCACTGCTTA-3') and reverse (CHD7-RT-R: 5'-ATCTATTTCATCTTTGAACGGTGT-3') primers. The PCR products were resolved on a 1% agarose gel and subsequently subjected to Sanger sequencing.

Homology modeling of human CHD7

Sequence similarity analysis revealed that the splice-site variant c.5405-17 G>A leads to an insertion within the DNA-binding domain (DBD) of CHD7 (CHD7-DBD). Therefore, only the truncated sequence encoding CHD7-DBD, rather than the full-length sequence of CHD7, was used for homology modeling using the SWISS-MODEL web server (https://swissmodel.expasy.org/). Both sequence and structural similarities were considered during template selection, and the DBD of yeast CHD1 was finally selected as the template for comparative modeling. Structural visualization was performed using PyMOL and the APBS web server (https://server.poissonboltzmann.org/).

Results

Clinical presentation

A 28-year-old female patient presented to our hospital with primary amenorrhea. She was the first and only child of a primigravida mother, delivered at approximately 8+ months of gestation via unattended home birth following prolonged labor for more than one day (exact duration unknown). The patient had a birth weight of over 2,500 g, and her length was comparable to that of her peers. Neonatal complications included a hoarse cry and weak vocalization. Torticollis and malformations of the right external ear were observed at birth, and the patient subsequently underwent reconstructive surgery of the right ear. Her postnatal course was marked by complications, including persistent diarrhea lasting 8 months and anemia requiring blood transfusion. She was breastfed until 2 years of age, and teething was noted around 1 year of age. The patient began walking independently at approximately 3 years of age, with verbal communication emerging at the same age. She exhibited signs of impaired hearing and cognition throughout her childhood. The patient also showed pronounced deficits in expressive language skills during the kindergarten period, accompanied by relatively poor motor coordination, evidenced by difficulty in activities such as dancing.

She sought evaluation at a different hospital at the age of 18 years due to absent pubertal development. Examinations at the previous medical institution revealed a normal karyotype (46, XX) and a possible empty sella turcica on pituitary magnetic resonance imaging. Pituitary amenorrhea was diagnosed based on sex hormone evaluation and thyroid function tests, although the specific data are not available. Bilateral breast development and intermittent menstrual cycles were achieved following treatment with estradiol valerate and progesterone; however, discontinuation of therapy one year prior resulted in amenorrhea. Her family history was unremarkable, with both parents exhibiting normal development, no consanguinity, and no similar medical conditions.

Physical examination revealed a height of 150.0 cm, a weight of 49.0 kg, and a body mass index of 21.8 kg/m^2. Notable features included facial asymmetry, bilateral low-set ears, right-sided microtia, and bilateral shortening of the 4th and 5th metacarpals (**Figure 2A-C**). The patient also exhibited severe bilateral hearing loss, absence of both pubic and axillary hair, chest deformity, and S-shaped scoliosis.

Evaluation of her endocrine profile at our institution revealed hypogonadotropic hypogonadism (**Table 1**), and echocardiography demonstrated a bicuspid aortic valve. Middle ear function testing (tympanometry, 226 Hz) revealed bilateral single-peaked tympanograms. Middle ear volume (right ear 1.19 ml, left ear 1.03 ml) and static acoustic admittance (bilaterally 0.71 ml) were within normal limits; however, middle ear pressure was significantly negative (right ear -121 daPa, left ear -145 daPa), indicating bilateral eustachian tube dysfunction and insufficient middle ear aeration. Acoustic reflex testing demonstrated that ipsilateral and contralateral acoustic reflexes were absent bilaterally (threshold >105 dB HL), suggesting impaired middle ear sound conduction or concurrent cochlear or retrocochlear auditory pathway abnormalities. Computed tomography (CT) of the temporal bone revealed a hypo-

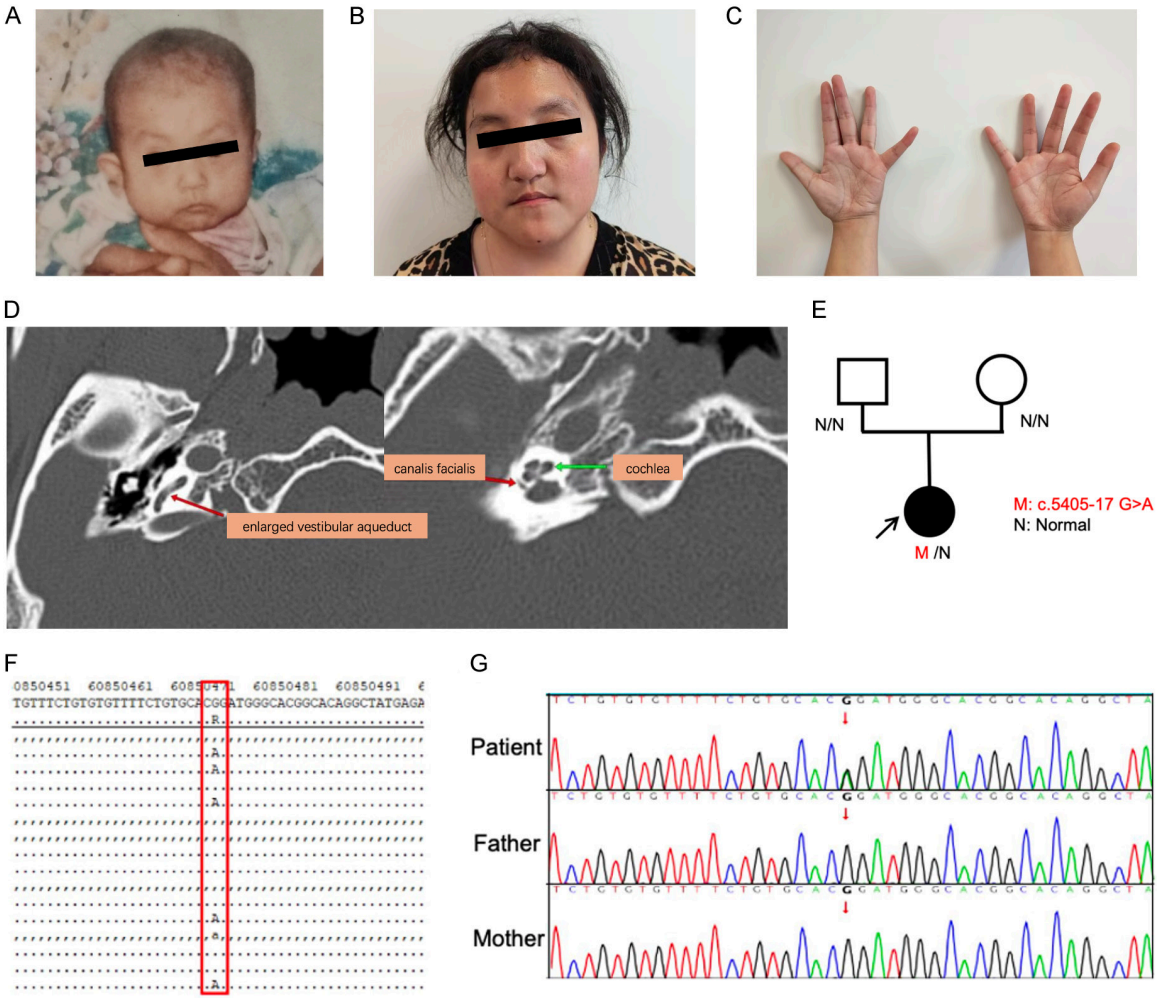

Figure 2. Clinical features, pedigree analysis, and genetic findings. A. Clinical photograph of the patient as a child. B. Clinical photograph of the patient at the time of evaluation in this study. C. Bilateral shortening of the 4th and 5th metacarpals. D. A hypoplastic vestibule, absent semicircular canals, and an enlarged vestibular aqueduct in computed tomography (CT). E. Pedigree map of the affected family. F. Identification of the heterozygous intronic variant c.5405-17G>A (NC_000008.11) in the *CHD7* gene. G. Validation of the *CHD7* variant in the parents by Sanger sequencing.

plastic vestibule, absent semicircular canals, and an enlarged vestibular aqueduct (**Figure 2D**), while nasopharyngolaryngoscopy demonstrated a deviated nasal septum.

Identification of de novo CHD7 variant

WES and bioinformatics analyses were performed for identifying potential genetic variants in the patient. The *de novo* variants were identified in a gene associated with CS following variant annotation and filtering using a customized WES panel. Specifically, the proband harbored a heterozygous *CHD7* splice variant that disrupted the acceptor splice site. No other potentially pathogenic single-nucleotide variants or copy number variations were detected in the genes potentially associated with CS. The pathogenicity of the variant was further confirmed using the Human Splicing Finder software.

The proband and her parents subsequently underwent DNA analysis by Sanger sequencing to assess the presence of the splice-site variant c.5405-17 G>A (**Figure 2F**, **2G**). The results confirmed that the proband harbored a heterozygous mutation, which was absent in both her parents, indicating a WT genotype (**Figure 2E-G**).

Functional impact of CHD7 splice-site alteration

The functional consequence of the *de novo* *CHD7* splice-site variant, c.5405-17 G>A, was

Table 1. Laboratory test data of the patient

Test items	Measured values	Reference ranges
Alkaline phosphatase (U/L)	74.00	43.00-136.00
Total bilirubin (μmol/L)	9.20	0.10-28.00
Direct bilirubin (μmol/L)	2.30	0.10-8.90
Alanine aminotransferase (U/L)	41.50	0.10-40.00
Aspartate aminotransferase (U/L)	27.40	0.10-40.00
Serum creatinine (μmol/L)	40.80	17.70-106.00
Serum uric acid (μmol/L)	322.60	90.00-420.00
Fasting blood glucose (mmol/L)	4.61	3.50-6.10
Serum sodium (mmol/L)	141.40	136.0-146.0
Serum potassium (mmol/L)	3.88	3.50-5.50
Serum chloride (mmol/L)	105.10	96.0-108.0
Serum calcium (mmol/L)	2.50	2.10-2.80
Serum phosphorus (mmol/L)	1.22	0.80-1.65
Serum magnesium (mmol/L)	1.09	0.66-1.07
Carbon Dioxide Combining Power (mmol/L)	27.50	20.00-30.00
Total cholesterol (mmol/L)	5.75	3.50-6.10
Triglyceride (mmol/L)	3.17	0.50-1.88
High density lipoprotein cholesterol (mmol/L)	1.49	0.80-1.89
Low density lipoprotein cholesterol (mmol/L)	3.72	0.00-3.40
Serum cortisol (nmol/L) (10am)	168.00	171.00-536.00
Adrenocorticotropic hormone (pg/ml) (10am)	7.67	7.20-63.30
Free thyroxine (pmol/L)	17.40	12.0-22.0
Free triiodothyronine (pmol/L)	6.80	3.10-6.80
Thyrotropin (μIU/ml)	2.15	0.270-4.200
Testosterone (nmol/L)	0.87	0.38-1.97
Estradiol (pmol/L)	78.00	81.90-1251.00 luteal phase 18.40-505.00 menopause 45.40-854.00 follicular phase 151.00-1461.00 ovulatory phase
Progesterone (nmol/L)	<0.159	5.82-75.90 luteal phase 0.00-0.40 menopause 0.18-2.84 follicular phase 0.39-38.10 ovulatory phase
Prolactin (uIU/ml)	152.00	102.00-496.00
Follicle-stimulating hormone (mIU/ml)	0.49	1.70-7.70 luteal phase 25.80-134.80 menopause 3.50-12.50 follicular phase 4.70-21.50 ovulatory phase
Luteinizing hormone (mIU/ml)	<0.300	1.00-11.40 luteal phase 7.70-58.50 menopause 2.40-12.60 follicular phase 14.00-95.60 ovulatory phase
β-human chorionic gonadotropin (mIU/ml)	<0.200	0.000-5.000

evaluated using a minigene assay, which demonstrated a 15-nt insertion in the MT region (**Figure 3A** and **3B**). Subsequent PCR amplification and agarose gel electrophoresis of the empty vector, WT, and MT constructs revealed distinct banding patterns corresponding to three discrete fragments (**Figure 3C**). Sanger sequencing of the WT and MT cDNA constructs yielded two distinct sequences (**Figure 3D**).

A 378-bp fragment was observed in the WT control, encompassing the complete sequenc-

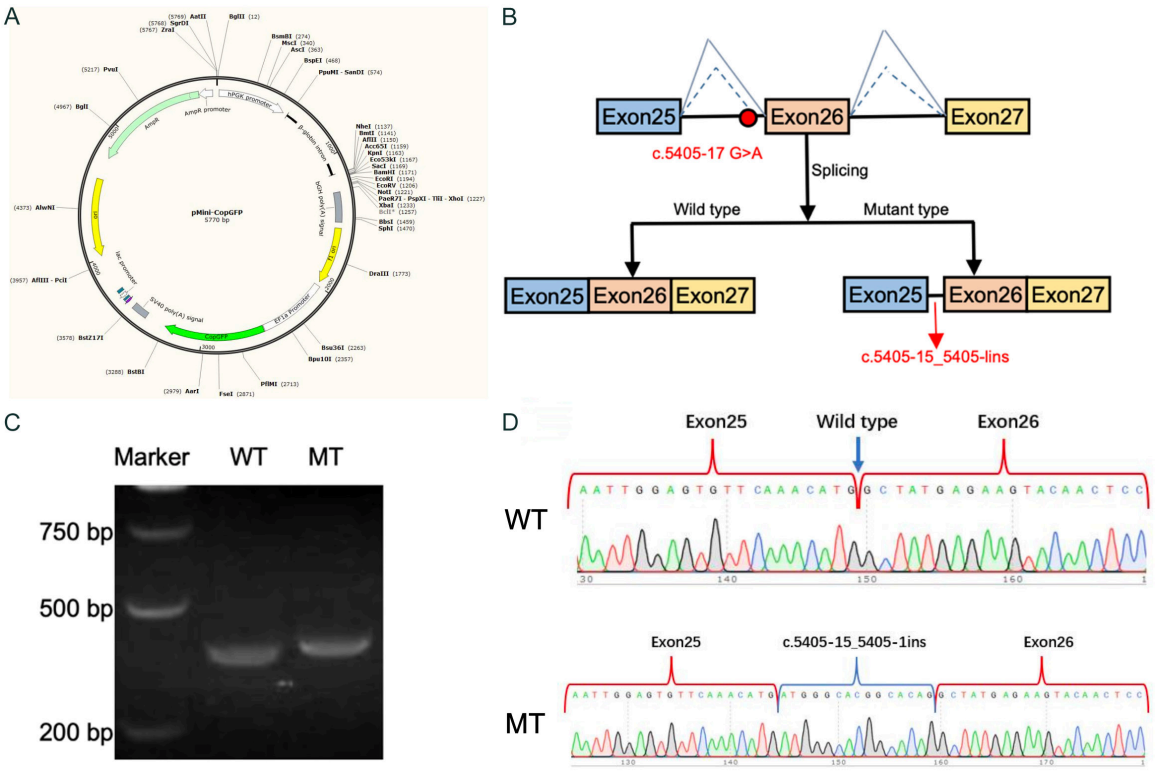

Figure 3. Minigene-based functional analysis of *CHD7*. A. Map of the pMini-CopGFP vector. B. Schematic representation of the exon-trapping vector containing the cloned *CHD7* fragment spanning exon 25-intron 25-exon 26-intron 26-exon 27. C. PCR-based amplification of cDNA fragments using specific primers, followed by visualization on a 1% agarose gel (WT = 378 bp, MT = 393 bp). D. Sanger sequencing of WT and MT splicing reporter minigenes.

es of exons 25, 26, and 27. In contrast, the MT variant exhibited a 393-bp fragment containing a 15-nt insertion resulting from the activation of a cryptic splice site within exon 26, leading to an in-frame insertion of five amino acids, p.(His1801_Gly1802insAspGlyHisGlyThr).

Homology modeling of human CHD7

The structural effects of the insertion caused by the splice-site mutation on human CHD7 protein were evaluated through characterization and comparison of the three-dimensional structures of WT and MT CHD7 proteins generated through homology modeling using the SWISS-MODEL web server (**Figure 4A** and **4B**). The c.5405-17 G>A substitution occurs within a recurrent intronic hotspot and creates a novel acceptor splice site that may functionally supersede the canonical acceptor site. This aberrant splicing event generates an mRNA transcript encoding a CHD7 variant with an in-frame insertion, 1801insDGHGT-CHD7. The resulting protein contains a five-amino-acid insertion positioned between the helicase and SANT domains of CHD7 (**Figure 4C**), which are located in the DBD.

Structural comparison and characterization of the WT and MT CHD7 proteins revealed that the five-amino-acid insert in the 1801insDGHGT-CHD7 variant disrupts the local side-chain architecture, increasing the distances between adjacent side chains beyond the typical range observed in proteins. The affected region lies within the SANT-SLIDE domain and is positioned between two alpha-helices in a tightly packed structural environment (**Figure 4A** and **4B**). Comparison of the structures of the WT and insertion variant of CHD7-DBD revealed that the principal differences are localized to two loop regions, designated L1 and L2. This insertion occurs within the L1 loop and induces conformational alterations in L2 (**Figure 5A** and **5B**). Comparison of the electrostatic surface potential of the insertion variant and the WT CHD7 protein revealed significant alterations in the insertion variant, which likely influence CHD7-DNA binding (**Figure 5C** and **5D**).

Therapeutic management and follow-up

The clinical management of CS is predominantly achieved through a multifaceted approach, as patients with CS typically present with a

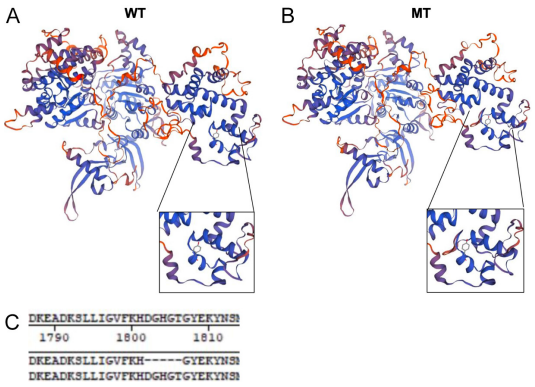

Figure 4. Homology modeling of human CHD7 using SWISS-MODEL. Three-dimensional structures of (A) WT and (B) MT CHD7 proteins in ribbon representation. (C) Sequence alignment of the CHD7-DBD of WT and MT proteins.

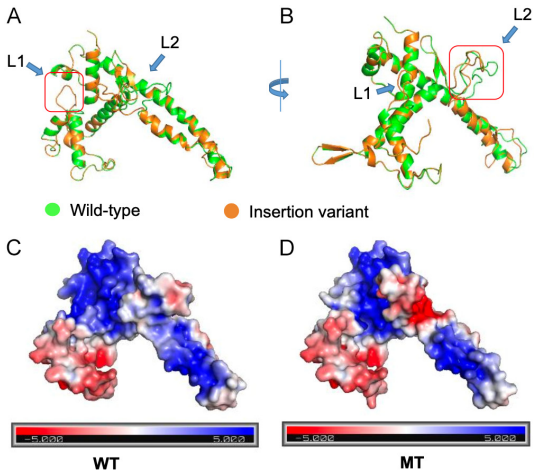

Figure 5. Structural comparison of WT and MT human CHD7 proteins. Three-dimensional structures of the (A) WT and (B) insertion variant of CHD7-DBD. The major structural differences are localized to two loops, designated L1 and L2, with the insertion occurring in L1. Electrostatic surface representation of the (C) WT and (D) insertion variant of CHD7-DBD.

diverse range of clinical manifestations, such as gonadal dysgenesis, short stature, and significant hearing impairment. Based on a comprehensive understanding of the disorder, parents of individuals affected with CS may prioritize the management of gonadal dysgenesis as a primary therapeutic focus.

Following comprehensive clinical evaluation in this study, the patient was initiated on hormone replacement therapy with Femoston tablets containing estradiol and dydrogesterone at a dose of 1 mg once daily. Consistent adherence to the prescribed regimen was followed by cyclical vaginal bleeding; however, her family opted against hearing-related interventions, despite the presence of some residual hearing capacity.

Discussion

The CHD7 protein belongs to the chromodomain helicase DNA-binding (CHD) family of proteins, which represent a highly conserved family of nuclear proteins with ATP-dependent chromatin remodeling activity [17]. CHD7 has critical contributions to the precise regulation of gene transcription during the initial stages of tissue development [18]. Notably, previous studies have demonstrated that CHD7 binds multiple chromatin loci, and that its binding profile is frequently associated with specific subsets of methylated histone H3 marks [19]. Earlier reports have additionally demonstrated that CHD7 primarily localizes to the nucleoplasm but is also present in the nucleolus, where it positively regulates the transcription of the 45S rRNA precursor [17].

Since the first genetically characterized case of CS was reported in China in 2014 [20], genetic analyses have been incorporated into numerous subsequent studies. Taken together, the findings of previous studies indicate that frameshift mutations represent the predominant class of *CHD7* mutations in Chinese patients [21]. The present study describes the case of a Chinese patient harboring a *CHD7* splice-site variant, c.5405-17G>A, which is predicted to affect mRNA splicing. Minigene assays provide a reliable approach for investigating splicing alterations, as they enable the direct cloning of PCR-amplified products derived from patient DNA into a modified vector.

The c.5405-17 G>A substitution is located within a recurrent intronic hotspot, and this variant generates a novel acceptor splice site, which may functionally compensate for the deficiencies of the canonical acceptor site. This results in an mRNA transcript encoding the 1801ins-DGHGT-CHD7 protein variant, which harbors a five-amino-acid insertion between the helicase and SANT domains. Brajadenta et al. reported that this CHD7 variant is nonfunctional and pathogenic [22]. Structural analysis of the WT and MT CHD7 proteins revealed that this substitution generates a truncated side chain at

this position, thereby disrupting the local hydrophobic interaction network. This disruption is attributed to the spatial separation between adjacent side chains exceeding the optimal range necessary for hydrophobic interactions. The results of computational structural analyses further indicated that the 1801insDGHGT-CHD7 variant is associated with perturbations in the local conformation, particularly in the region adjacent to the nucleotide-binding site. Notably, this perturbation is likely to cause a more pronounced effect on the inactive CHD7 variant than on its catalytically active form. The SANT domain has critical functions in the recognition of histone tails and the mediation of DNA binding. By conducting structural analyses, Bouazoune and Kingston [23] revealed that the inter-domain linker regions play critical roles in the maintenance of conformational flexibility required for ATP-dependent nucleosome remodeling. The computational analyses performed in this study suggested that the p. His1801_Gly1802ins insert modifies the local electrostatic potential and reorients the DNA-binding loops, which likely impair the efficiency of nucleosome mobilization by CHD7, thereby perturbing the transcriptional programing in neural crest cells [8, 24].

Collectively, the present investigation detected a c.5405-17 G>A splice-site mutation in a female patient from China with classical CS through WES. Minigene-based functional analyses demonstrated that this splice-site variant produces an aberrant transcript with a 15-bp in-frame insertion, resulting in the addition of five amino acids in the variant CHD7 protein. Notably, the observed improvement in patient survival emphasizes the significance of early diagnosis in CS, thereby facilitating timely and effective therapeutic interventions. The findings obtained herein provide key insights for genetic counseling and may assist the identification of optimum clinical interventions for patients with a definitive genetic basis of congenital syndromes.

Although the results of minigene-based functional evaluation provide critical insights, the present investigation has certain limitations, which are described hereafter. First, although the *in vitro* minigene system confirmed the splicing defect, it may not accurately reproduce the endogenous splicing ratios in specific human tissues. Second, although the study predicted the structural effects of the five-amino-acid insertion in CHD7 through computational analyses, direct functional validation at the protein level, such as chromatin-binding or ATPase activity tests, was not performed.

These findings collectively emphasize that future investigations on non-canonical splicing variants are necessary in patients presenting with clinical features of CS who are negative for coding-region mutations. In the future, studies should focus on optimizing the long-term clinical management of congenital endocrine manifestations, including the hypogonadotropic hypogonadism observed in the patient reported herein, and on elucidating the effects of specific domain insertions on chromatin remodeling mediated by CHD7. These insights are expected to advance our understanding of genotype-phenotype correlations in this complex congenital multisystem disorder.

Acknowledgements

The authors are sincerely grateful to the patient's family for their support and understanding.

Disclosure of conflict of interest

None.

Address correspondence to: Yangfan Fei, West China Hospital Sichuan University, Meishan Hospital, Meishan, Sichuan, China. ORCID: 0000-0002-0447-8672; E-mail: feiyangfan_mmph@163.com; Qinglian Zhang, School of Laboratory Medicine, Chengdu Medical College, Chengdu, Sichuan, China. ORCID: 0000-0003-1126-9470; E-mail: qlzhang80@163.com

References

[1] Hittner HM, Hirsch NJ, Kreh GM and Rudolph AJ. Colobomatous microphthalmia, heart disease, hearing loss, and mental retardation--a syndrome. J Pediatr Ophthalmol Strabismus 1979; 16: 122-128.

[2] Issekutz KA, Graham JM Jr, Prasad C, Smith IM and Blake KD. An epidemiological analysis of CHARGE syndrome: preliminary results from a Canadian study. Am J Med Genet A 2005; 133A: 309-317.

[3] Hall BD. Choanal atresia and associated multiple anomalies. J Pediatr 1979; 95: 395-398.

[4] Pagon RA, Graham JM Jr, Zonana J and Yong SL. Coloboma, congenital heart disease, and

choanal atresia with multiple anomalies: CHARGE association. J Pediatr 1981; 99: 223-227.
[5] Vissers LE, van Ravenswaaij CM, Admiraal R, Hurst JA, de Vries BB, Janssen IM, van der Vliet WA, Huys EH, de Jong PJ, Hamel BC, Schoenmakers EF, Brunner HG, Veltman JA and van Kessel AG. Mutations in a new member of the chromodomain gene family cause CHARGE syndrome. Nat Genet 2004; 36: 955-957.
[6] Zentner GE, Layman WS, Martin DM and Scacheri PC. Molecular and phenotypic aspects of CHD7 mutation in CHARGE syndrome. Am J Med Genet A 2010; 152A: 674-686.
[7] Basson MA and van Ravenswaaij-Arts C. Functional insights into chromatin remodelling from studies on CHARGE syndrome. Trends Genet 2015; 31: 600-611.
[8] Bajpai R, Chen DA, Rada-Iglesias A, Zhang J, Xiong Y, Helms J, Chang CP, Zhao Y, Swigut T and Wysocka J. CHD7 cooperates with PBAF to control multipotent neural crest formation. Nature 2010; 463: 958-962.
[9] Hargreaves DC and Crabtree GR. ATP-dependent chromatin remodeling: genetics, genomics and mechanisms. Cell Res 2011; 21: 396-420.
[10] Aramaki M, Udaka T, Kosaki R, Makita Y, Okamoto N, Yoshihashi H, Oki H, Nanao K, Moriyama N, Oku S, Hasegawa T, Takahashi T, Fukushima Y, Kawame H and Kosaki K. Phenotypic spectrum of CHARGE syndrome with CHD7 mutations. J Pediatr 2006; 148: 410-414.
[11] Bergman JE, Janssen N, Hoefsloot LH, Jongmans MC, Hofstra RM and van Ravenswaaij-Arts CM. CHD7 mutations and CHARGE syndrome: the clinical implications of an expanding phenotype. J Med Genet 2011; 48: 334-342.
[12] Janssen N, Bergman JE, Swertz MA, Tranebjaerg L, Lodahl M, Schoots J, Hofstra RM, van Ravenswaaij-Arts CM and Hoefsloot LH. Mutation update on the CHD7 gene involved in CHARGE syndrome. Hum Mutat 2012; 33: 1149-1160.
[13] Lalani SR, Safiullah AM, Molinari LM, Fernbach SD, Martin DM and Belmont JW. SEMA3E mutation in a patient with CHARGE syndrome. J Med Genet 2004; 41: e94.
[14] Dirix M, Gribouval O, Arrondel C, Benjelloun S, Boyer O, Charbit M, Antignac C, Heidet L and Dorval G. Overcoming the challenges associated with identification of deep intronic variants by whole genome sequencing. Clin Genet 2023; 103: 693-698.
[15] Rodriguez-Muñoz A, Liquori A, García-Bohorquez B, Jaijo T, Aller E, Millán JM and García-García G. Functional assays of non-canonical splice-site variants in inherited retinal dystrophies genes. Sci Rep 2022; 12: 68.
[16] Zhang X, Cai M, Ma Y, Chen J, Huang S, Cai M, Ding Y, Ma D, Gao Q, Hu X, Zhu C and Yi L. Minigene assay as an effective molecular diagnostic strategy in determining the pathogenicity of noncanonical splice-site variants in FLCN. J Mol Diagn 2023; 25: 110-120.
[17] Bergman JE, Janssen N, van der Sloot AM, de Walle HE, Schoots J, Rendtorff ND, Tranebjaerg L, Hoefsloot LH, van Ravenswaaij-Arts CM and Hofstra RM. A novel classification system to predict the pathogenic effects of CHD7 missense variants in CHARGE syndrome. Hum Mutat 2012; 33: 1251-1260.
[18] Schnetz MP, Bartels CF, Shastri K, Balasubramanian D, Zentner GE, Balaji R, Zhang X, Song L, Wang Z, Laframboise T, Crawford GE and Scacheri PC. Genomic distribution of CHD7 on chromatin tracks H3K4 methylation patterns. Genome Res 2009; 19: 590-601.
[19] Zentner GE, Hurd EA, Schnetz MP, Handoko L, Wang C, Wang Z, Wei C, Tesar PJ, Hatzoglou M, Martin DM and Scacheri PC. CHD7 functions in the nucleolus as a positive regulator of ribosomal RNA biogenesis. Hum Mol Genet 2010; 19: 3491-3501.
[20] Liu L, Yu T, Wang L, Mo X and Yu Y. A novel CHD7 mutation in a Chinese patient with CHARGE syndrome. Meta Gene 2014; 2: 469-478.
[21] Cheng SSW, Luk HM, Chan DKH and Lo IFM. CHARGE syndrome in nine patients from China. Am J Med Genet A 2020; 182: 15-19.
[22] Brajadenta GS, Bilan F, Gilbert-Dussardier B, Kitzis A and Thoreau V. A functional assay to study the pathogenicity of CHD7 protein variants encountered in CHARGE syndrome patients. Eur J Hum Genet 2019; 27: 1683-1691.
[23] Bouazoune K and Kingston RE. Chromatin remodeling by the CHD7 protein is impaired by mutations that cause human developmental disorders. Proc Natl Acad Sci U S A 2012; 109: 19238-19243.
[24] Hendricks EI and Liebl FLW. The CHD family chromatin remodeling enzyme, Kismet, promotes both clathrin-mediated and activity-dependent bulk endocytosis. PLoS One 2024; 19: e0300255.